JGR Space Physics

RESEARCH ARTICLE
10.1029/2021JA029694

Special Section:
Cluster 20th anniversary: results from the first 3D mission

Ion Convection as a Function of Distance to the Neutral Sheet in Earth's Magnetotail

Ghai Siung Chong[1], T. Pitkänen[1,2], M. Hamrin[1], and A. Schillings[1]

[1]Department of Physics, Umeå University, Umeå, Sweden, [2]Institute of Space Sciences, Shandong University, Weihai, China

Abstract We utilized 33 years of data obtained by the Geotail, THEMIS, Cluster and MMS missions to investigate the slow (<200 km/s) ion flows perpendicular to the magnetic field in Earth's magnetotail plasma sheet. By using plasma β as a proxy of distance to the neutral sheet, we find that the ion flow patterns vary systematically within the plasma sheet. Particularly, in regions farther from the neutral sheet, earthward (tailward) flows exhibit a strong tendency to diverge (converge) quasi-symmetrically, with respect to the midnight meridional plane. As the distance becomes closer toward the neutral sheet, this tendency to diverge and converge gradually weakens. Moreover, duskward flows become the dominant components in both the earthward and tailward flows. These variations in ion flow patterns with distance to neutral sheet are hemispherically independent. We suggest that the spatial profiles of the electric and diamagnetic drift vary with distance to the neutral sheet and are therefore responsible for the varying ion flow patterns.

Plain Language Summary The plasma sheet can be visualized as "layers" stacking on top of each other where the middle layer represents the neutral sheet. In this study, we investigate the plasma convection patterns in these various plasma sheet "layers" in terms of their location relative to the neutral sheet. Our study finds that the plasma convection patterns in the plasma sheet are different depending on their distance from the neutral sheet. Farther from the neutral sheet, earthward and tailward flows converge and diverge quasi-symmetrically, respectively, with respect to the midnight plane. As distance becomes closer to the neutral sheet, the degree of convergence and divergence weakens. At distance closest to the neutral sheet, duskward flows become the dominant components. We suggest that the spatial profiles of the electric and diamagnetic drift vary with distance to the neutral sheet and are therefore responsible for the varying ion flow patterns.

Key Points:

- Slow plasma sheet ion flows (<200 km/s) perpendicular to the magnetic field vary systematically with distance to the neutral sheet
- Farther from the neutral sheet, earthward (tailward) flows exhibit stronger flow divergence (convergence) with the midnight meridional plane
- Closer to the neutral sheet, the diverging/converging tendency weakens, and the flows are dominated by duskward flow components

Correspondence to:
G. S. Chong,
ghaisiung@gmail.com

Citation:
Chong, G. S., Pitkänen, T., Hamrin, M., & Schillings, A. (2021). Ion convection as a function of distance to the neutral sheet in Earth's magnetotail. *Journal of Geophysical Research: Space Physics*, *126*, e2021JA029694. https://doi.org/10.1029/2021JA029694

Received 18 JUN 2021
Accepted 10 NOV 2021

Author Contributions:
Conceptualization: Ghai Siung Chong, T. Pitkänen, M. Hamrin
Data curation: Ghai Siung Chong
Formal analysis: Ghai Siung Chong, T. Pitkänen
Investigation: Ghai Siung Chong, T. Pitkänen
Methodology: Ghai Siung Chong, T. Pitkänen, M. Hamrin
Resources: Ghai Siung Chong, T. Pitkänen, M. Hamrin
Software: Ghai Siung Chong
Supervision: T. Pitkänen, M. Hamrin
Validation: Ghai Siung Chong

1. Introduction

The Earth's magnetotail plasma sheet plays an important role in governing the energy, mass and momentum transport in the coupled magnetosphere-ionosphere system. The ion flows in the plasma sheet are highly dynamic and their properties have been extensively researched. Previous studies have primarily focused on (a.) fast and slow flows (Angelopoulos et al., 1994, 1992; Baumjohann et al., 1990; Juusola, Østgaard, & Tanskanen, 2011; Raj et al., 2002; Zhang, Wang, et al., 2015), (b.) perpendicular and field-aligned flows (Baumjohann et al., 1988; Decoster & Frank, 1979; Raj et al., 2002; Takahashi & Hones, 1988), (c.) earthward and tailward flows (Juusola, Østgaard, & Tanskanen, 2011; Zhang, Baumjohann, et al., 2015; Ohtani et al., 2009; Schödel, Nakamura, et al., 2001), (d.) distant-tail and near-Earth flows (Ohtani et al., 2009; Schödel, Baumjohann, et al., 2001; Nakamura et al., 1994), as well as (e.) the dependence on external environments, for instance, on the orientation of the interplanetary magnetic field (Pitkänen et al., 2019; Wang et al., 2006), and on substorms and steady magnetospheric convection (Juusola, Østgaard, Tanskanen, Partamies, & Snekvik, 2011; McPherron et al., 2011). In brief, these studies point toward that the plasma behaviors in the different regions within the plasma sheet can vary significantly under various environments.

However, it is yet to be established how the ion flows perpendicular to the magnetic field depend on the distance to the neutral sheet. In general, the perpendicular ion flows in the plasma sheet can be described by the combined effects of the energy-independent electric and energy-dependent diamagnetic drift (Angelopoulos et al., 1993; Baumjohann et al., 1988; Hori et al., 2000; Juusola, Østgaard, & Tanskanen, 2011; Kissinger et al., 2012; Paterson et al., 1998; Pitkänen et al., 2019; Wang et al., 2006). One common observation among these studies is a dawn-dusk asymmetry in the average flows in the plasma sheet. That is, on average, there are more duskward than dawnward flows. However, the degree of this dawn-dusk asymmetry differs from study to study. For instance, by utilizing 0.5 as a lower limit of plasma β (ratio of ion thermal pressure to magnetic pressure) in identifying the

Visualization: Ghai Siung Chong, T. Pitkänen, M. Hamrin
Writing – original draft: Ghai Siung Chong
Writing – review & editing: Ghai Siung Chong, T. Pitkänen, M. Hamrin, A. Schillings

plasma sheet, the dominance of duskward flows in Angelopoulos et al. (1993); Juusola, Østgaard, and Tanskanen (2011) is more prominent (by eye inspection) when compared to Zhang, Wang, et al. (2015) which utilized 0.1 as a lower limit of plasma β. While the utilized missions vary, these studies have implemented different lower limits on plasma β, among other criteria, in identifying the plasma sheet. On the basis that the value of plasma β increases from the boundary regions, through the plasma sheet to the neutral sheet (Baumjohann et al., 1988; Boakes et al., 2014; Zhang, Baumjohann, et al., 2015), these studies hint that the plasma flows in the plasma sheet differ depending on the distance to the neutral sheet.

Therefore, in this study, we take advantage of a large database of *in-situ* spacecraft data (~33 years), to report how the average perpendicular ion flows vary within the plasma sheet with ranging distance to the neutral sheet. We will also discuss how the balance between electric and diamagnetic drifts can contribute to such variations.

2. Instrumentation

In this study, the magnetic field and ion data (no differentiation between species) of magnetotail plasma sheet data are obtained from the Geotail, Time History of Events and Macroscale Interactions during Substorms (THEMIS), Cluster and Magnetospheric Multiscale (MMS) missions. The descriptions of the different utilized instruments are summarized in Table 1. The geocentric solar magnetospheric (GSM) coordinate system is used throughout this study.

3. Data Selection

In this study, all ion flow data samples that satisfy the following criteria are considered. Spatially, all nightside ion flows (i.e., $X < 0\ R_E$) are considered. A criterion of $B_z > 3$ nT is implemented to exclude ions that are associated with magnetic plasmoids tailward of the reconnection sites (Hones, 1979; Nagai et al., 1998). To remove possible magnetosheath data samples, we implement that the ratio between ion temperature and ion number density, T_i/n_i, must be higher than 1,000 eV/cm^{-3}, in line with previous studies (Hamrin et al., 2009; Hori et al., 2000; Nilsson et al., 2016; Pitkänen et al., 2019). Only ion flow data with its velocity component perpendicular to the magnetic field, $|\mathbf{V}_\perp|$ smaller than 200 km/s are considered. This criteria should effectively exclude the high-speed (i.e., >250 km/s) convective bursty bulk flows (Angelopoulos et al., 1992, 1994; Baumjohann et al., 1990) in the plasma sheet. These transient disturbances have characteristic properties and they are not representative of the average slow flows in the plasma sheet.

A plasma ion β threshold of 0.025 is chosen as a lower limit for the outer plasma sheet (Boakes et al., 2014). This choice of low plasma β is discussed in Section 3.1. This is to remove possible plasma from the lobe and boundary region with low β. In addition, ion flow data with $V_{\perp x} > 0$ km/s and $V_{\text{tot, x}}$ (total velocity) >0 km/s are considered earthward flows. Ion flow data with $V_{\perp x} < 0$ km/s and $V_{\text{tot, x}} < 0$ km/s are considered tailward flows. Note that this categorization of ion flows is solely based on the signs of the X-component, regardless of the magnitude of Y and Z-components. Furthermore, no criterion on the duration/continuity is implemented on the flow samples. That is, each data sample is selected on an individual basis, regardless if they are part of "blocks" of flows (either earthward or tailward).

In Figures 1a–1d, we show the total spacecraft observation time (color scale) across all missions of earthward (~771 days) and tailward (~350 days) ion flows with criteria mentioned above in a $2 \times 2\ R_E$ grid in the XY and YZ planes. We also overplot the average earthward and tailward $\mathbf{V}_\perp$ in Figures 1a–1d. Since different plasma instruments have different sampling time durations, the averaged velocity vectors throughout the study are weighted by the respective sampling times (T_s):

$$\bar{V}_{x,y,z} = \frac{\sum_{i=1}^{n} T_{s,i} V_{x,y,z}}{\sum_{i=1}^{n} T_{s,i}} \quad (1)$$

This approach is similar to previous works which utilize similar data set (e.g., Pitkänen et al., 2019). Note that in the YZ planes in Figures 1b and 1d, only ion flows at $X <- 10\ R_E$ are considered.

Table 1
Descriptions of the Geotail, THEMIS, Cluster, and MMS Missions We Utilize in This Study

Missions	Date range	Data resolution		Ion energy range
		Magnetic field (s)	Ion moment (s)	
Geotail[a,b]	January 1995–December 2006	~3	~12	few eV/q–43 keV/q
THEMIS		~3	~3	1.6 eV/q–25 keV/q
A	January 2008–December 2009			
B	November 2007–December 2009			
C	August 2007–December 2009			
D	August 2007–December 2009			
C	August 2007–December 2009			
Cluster 3	January 2001–December 2009	~4	~4	5 eV/q–32 keV/q
MMS 1	January 2017–December 2020	~0.062 5	~4.5	10 eV/q–30 keV/q

Note. The magnetic field and the ion data are obtained from the following instruments. Geotail: Magnetic Field Experiment (MGF; Kokubun et al., 1994) and the Low Energy Particle Experiment (LEP; Mukai et al., 1994). THEMIS: Fluxgate Magnetometer (FGM; Auster et al., 2008) and the ElectroStatic Analyzer (ESA; McFadden et al., 2008). Cluster: Fluxgate Magnetometer (FGM) (Balogh et al., 2001) and the Hot Ion Analyzer (HIA; Rème et al., 2001). MMS: Fluxgate Magnetometers (FGM; Russell et al., 2016) and the Fast Plasma Investigation (FPI; Pollock et al., 2016).
[a]Only Editor-A data are used. [b]B_z offset correction is applied on Geotail's magnetic field data.

Observable from Figures 1a and 1c, our data selection criteria exclude the non-plasma sheet data quite effectively. For instance, the total observation time within the geostationary orbit (gray circle) and the flows outside the nominal magnetopause (gray curve) is very low (≪1 hr per bin).

The average earthward and tailward flow patterns in the XY plane presented in Figures 1a and 1c are consistent with previous studies (e.g., Angelopoulos et al., 1993; Hori et al., 2000; Juusola, Østgaard, & Tanskanen, 2011; Kissinger et al., 2012; Paterson et al., 1998; Pitkänen et al., 2019; Wang et al., 2006): earthward flows diverge quasi-symmetrically from the midnight meridional plane (i.e., $Y \approx 0\ R_E$). In a similar but inversed manner,

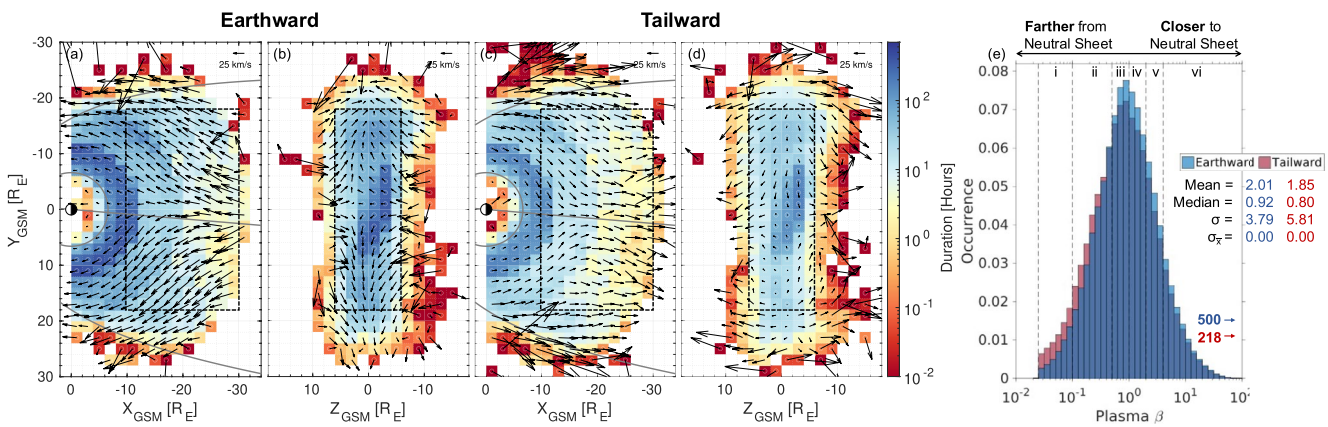

Figure 1. The total spacecraft observation time in the XY and YZ planes for (a–b) earthward ($\mathbf{V}_{\perp x} > 0$ km/s & $\mathbf{V}_{\text{tot, x}} > 0$ km/s) and (c–d) tailward flows ($V_{\perp x} < 0$ km/s & $\mathbf{V}_{\text{tot, x}} < 0$ km/s) respectively. $\mathbf{V}_\perp$ is the velocity component perpendicular to the magnetic field. For YZ planes in (b) and (d), additional criterion of $X < -10\ R_E$ is implemented. The color bars show the total spacecraft observation time in hours (log-scale) in each bin. The average earthward and tailward $\mathbf{V}_\perp$ are overplotted in (a–d) respectively. The geostationary orbit at the 6.6 R_E radial distance is illustrated by a gray circle. The nominal magnetopause (Shue et al., 1997, with dynamic pressure of 1 nPa and IMF B_z of 0 nT) is illustrated by a gray curve. Both the Sun-Earth line and the nominal magnetopause have been rotated 4.8° clockwise (to account for the solar wind aberration; see Juusola, Østgaard, and Tanskanen (2011)). The dashed rectangles in (a–d) indicate the "effective plasma sheet," outlined by $-30\ R_E \le X < -10\ R_E$, $|Y| < 18\ R_E$ and $|Z| < 6\ R_E$ respectively. See main texts for more information. The high spacecraft observation time at radial distance <12 R_E in (a) and (c) is primarily due to the higher sampling frequency by THEMIS a, d and e missions. (e) The distribution of plasma β for earthward (blue-colored) and tailward (red-colored) flows respectively. The number of data points that are not included (due to the *X*-axis limit) are noted on the lower right corner of the respective histograms. Regions of overlapped histograms are shaded in dark blue. σ and $\sigma_{\bar{x}}$ represent the standard deviation and standard error. The occurrence is normalized with respect to the relative probability, so that the sum of the occurrences over all binned variables equals 1. Subscripts *i-vi* correspond to the classification of plasma β in Figures 2–4. See main texts for more information.

tailward flows converge quasi-symmetrically toward the midnight meridional plane. For simplicity, midnight meridional plane will be referred to just 'midnight plane' hereon. On average, both earthward and tailward flows are weakly dominated by duskward flows. It is this weak dominance of duskward flows that gives rise to the dawn-dusk asymmetry of the average ion flows. The flow divergence and convergence with respect to the midnight plane for earthward and tailward flows are also observable in the YZ plane (Figure 1b and d). The weak dominance of duskward flows is also evident in the YZ plane, that is $|+V_{\perp y}|$ is generally larger than $|-V_{\perp y}|$. Earth's magnetic field configuration in the magnetotail is dipolar and highly stretched. This configuration can explain the flow convergence and divergence from $Z = 0\ R_E$ for earthward and tailward flows respectively, as observable in the YZ plane. In this study, when describing the flow behaviors in a plane, flow divergence from (convergence toward) a particular axis implies that the velocity vectors in the plane generally point away from (toward to) that particular axis.

3.1. Plasma β as a Proxy of Distance to the Neutral Sheet

In this study, we investigate the average ion flow patterns as a function of distance to the neutral sheet. To do this, we vary the plasma β as a proxy of distance to the neutral sheet. The plasma β is divided into six categories where the distance ranges from "farther from the neutral sheet" to "closer to the neutral sheet" as following: (a) $0.025 < \beta \leq 0.1$, (b) $0.1 < \beta \leq 0.5$, (c) $0.5 < \beta \leq 1$, (d) $1 < \beta \leq 2$, (e) $2 < \beta \leq 4$, and (f) $4 < \beta$. In this study, we visualize the plasma sheet as 2D "layers" in the XY plane. The middle layer represents the neutral sheet separating the Northern (top layers) and Southern (bottom layers) plasma sheet. Therefore, in this study, "farther from" and "closer to" the neutral sheet can be visualized as varying distance with respect to the neutral sheet along the Z-axis (north-south axis).

We show the distributions of plasma β for earthward (blue-colored) and tailward (red-colored) flows in Figure 1e. The categorizations of plasma β described above are also reflected in Figure 1e by dashed-lines. The corresponding roman numerals $i \rightarrow vi$ mark the distance from "farther from" to "closer to" the neutral sheet. Observable from Figure 1e, both earthward and tailward flows do not have distinctive difference in term of the distribution of plasma β.

The distribution of plasma β in the plasma sheet has an increasing gradient with radial distance from Earth up to $\approx 10\ R_E$ in the nightside. Beyond a radial distance of $10\ R_E$, the spatial profile of plasma β is rather homogeneous (see Juusola, Østgaard, & Tanskanen, 2011). Therefore, the ion category with low plasma β at radial distance $<10\ R_E$ can include the near-Earth plasma sheet ion. These data do not represent ions at distance farther from the neutral sheet. To exclude (a) these near-Earth plasma sheet data, (b) the ion samples within the geostationary orbit, and (c) the ion samples outside the nominal magnetopause, we only consider ions in the region outlined by $-30\ R_E \leq X < -10\ R_E$, $|Y| < 18\ R_E$ and $|Z| < 6\ R_E$ as the "effective plasma sheet." See the dashed rectangle in Figures 1a–1d for the outlines. Only the ions in this region will be considered in the following quantitative analyses.

By using data from the Cluster mission, Boakes et al. (2014) indicate that the lower limit of plasma β for plasma sheet ion is 0.01. Haaland et al. (2017) utilized plasma β of 0.05 as a higher limit of the magnetotail lobes. Therefore, the ion category with low plasma β (i.e., $0.025 < \beta \leq 0.1$) may include data samples from the lobes. However, we emphasize that, even if the category of ions with plasma $\beta \leq 0.1$ are not considered, our results on the variations in ion flow patterns with distance to the neutral sheet (see Section 4) will not be affected.

4. Results

In Figure 2, we show the distribution of (a–b) earthward and (c–d) tailward $\mathbf{V}_\perp$ in the XY and YZ planes for ranging distance to the neutral sheet. Subscripts $i \rightarrow vi$ (left to right) correspond to distance that ranges from "farther from" to "closer to" the neutral sheet. The color bars in (a and c) show $\tan^{-1}(V_{\perp y}/|V_{\perp x}|)$ where the resolved angle ranges from $-90°$ (blue-dawnward) to $+90°$ (red-duskward). The color bars in (b and d) show $V_{\perp y}$ where blue (red) indicates dawnward (duskward) flows. In brief, lighter (darker) shades of colors indicate weaker (stronger) flow deviation from the midnight plane.

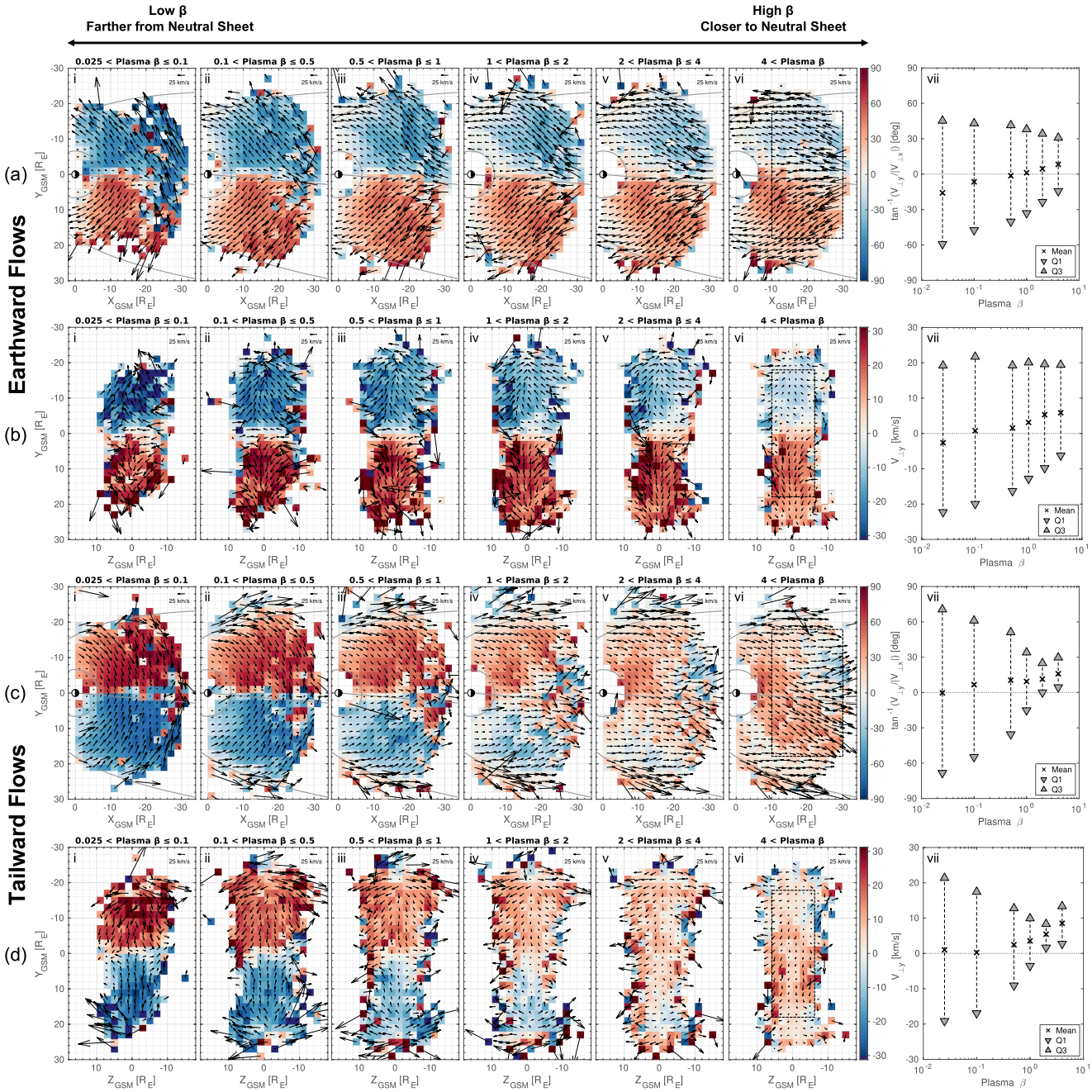

Figure 2. The distribution of (a–b) earthward and (c–d) tailward $\mathbf{V}_{\perp}$ in the XY and YZ planes respectively for ranging distance to the neutral sheet. Note that the *X* and *Y*-axes of the XZ planes in (b and d) show the Z and Y GSM-coordinates respectively. Subscripts *i-vi* (left to right) denotes the distance that ranges from "farther from the neutral sheet" to "closer to the neutral sheet." This classification of ranging distance to the neutral sheet is based on plasma β, where subscripts *i-vi* correspond to Figure 1e. See Section 3.1 for more information. The vectors represent $\mathbf{V}_{\perp}$. The color bars in (a and c) show $\tan^{-1}(V_{\perp y}/|V_{\perp x}|)$ while the color bars in (b and d) show $V_{\perp y}$. For YZ planes in (b and d), only ion flows at $X < -10\ R_E$ are considered. The right-hand most panels (*vii*) in (a and c) show the mean $\tan^{-1}(V_{\perp y}/|V_{\perp x}|)$ computed from respective *i-vi* in the region outlined by $-30\ R_E \leq X < -10\ R_E$ and $|Y| < 18\ R_E$ (as illustrated by the dashed rectangle in *vi*). The right-hand most panels (*vii*) in (b)&(d) show the mean $V_{\perp y}$ computed from respective *i-vi* in the region outlined by $|Y| < 18\ R_E$ and $|Z| < 6\ R_E$ (as illustrated by the dashed rectangle in *vi*). The downward and upward triangles denote the first (Q1) and third (Q3) quartile of the distribution.

4.1. XY Plane

Earthward flows: Using plasma β as a proxy, at distance farthest away from the neutral sheet (Figure 2ai), the flow vectors strongly diverge from the midnight plane and dawnward flows are more dominant. This is seen as the grids are dominated by darker shades of colors and there are more blue than red-shaded grids. As the

distance becomes closer to the neutral sheet (Figure 2ai–vi), the strength of the divergence from the midnight plane gradually weakens and duskward flows become the dominant components. This is reflected as the overall colored grids vary from darker to lighter shades and there are more red than blue-shaded grids. In addition, the decrease in dawnward flow strength is notably more apparent when compared to the decrease in duskward flow strength. That is, blue-colored grids vary from darker to lighter shades more significantly when compared to the red-colored grids.

We illustrate these variations in flow patterns quantitatively in Figure 2a-vii. Figure 2a-vii shows the mean angle $\tan^{-1}(V_{\perp y}/|V_{\perp x}|)$ computed from the "effective" plasma sheet region outlined by the dashed rectangle illustrated in (a)-*vi*. As plasma β increases, the mean angle changes from primarily dawnward to primarily duskward and the interquartile range (Q3-Q1) narrows considerably. In brief, as distance becomes closer to the neutral sheet, duskward flows become the dominant components and the strength of the flow divergence from the midnight plane weakens.

Tailward flows: The variation in tailward flow patterns is somewhat similar but opposite to those of earthward flow patterns. As distance becomes closer to the neutral sheet (Figure 2c, i–vi), the strength of the flow convergence toward the midnight plane gradually weakens and duskward flows become the dominant components. In fact, at distance closest to the neutral sheet (Figures 2cv–vi), duskward flows are so dominant that the converging property of tailward flows is no longer observable. It is noteworthy to mention that at distance farthest from the neutral sheet (Figure 2ci), tailward flows converge quasi-symmetrically toward the midnight plane. This is in contrast to the earthward flows which have a weak dominance in dawnward flows in the same proxy of distance (Figure 2ai).

Similar to earthward flows, we illustrate this variation in flow patterns quantitatively in Figure 2cvii. For instance, as plasma β increases, the mean angle $\tan^{-1}(V_{\perp y}/|V_{\perp x}|)$ changes from zero to primarily duskward and the interquartile range (Q3-Q1) narrows considerably. In fact, at distance closest to the neutral sheet (Figure 2cvi), both Q3 and Q1 are in the duskward regime. This indicates that the tailward flows near the neutral sheet are dominantly duskward (more dominant than the earthward flows in the same proxy of distance, see Figure 2avi).

Summary: For both earthward and tailward flows, as the distance becomes closer to the neutral sheet, duskward flows become the dominant components and the strength of the flow deviation from the midnight plane weakens.

4.2. YZ Plane

Earthward flows: In the YZ plane, as distance becomes closer to the neutral sheet (Figure 2bi–vi), the overall colored grids vary from darker to lighter shades. This indicates that the strength of the dawn-dusk flow component gradually weakens. That is, the flow deviation from the midnight plane gradually weakens. Furthermore, the decrease in dawnward flow strength is notably more apparent when compared to the decrease in duskward flow strength. That is, blue-colored grids vary from darker to lighter shades more significantly when compared to the red-colored grids. We illustrate this variation in flow patterns quantitatively in Figure 2b-vii. Figure 2b-vii shows the mean $V_{\perp y}$ computed from the region outlined by the dashed rectangle illustrated in (b)-*vi*. Observable from Figure 2bvii, as plasma β increases, the mean $V_{\perp y}$ changes from zero to primarily duskward and the interquartile range (Q3-Q1) narrows.

Tailward flows: As distance becomes closer to the neutral sheet (Figure 2di–vi), the overall colored grids vary from darker to lighter shades and there are more red than blue-shaded grids. This indicates that the flow deviation from the midnight plane gradually weakens and duskward flows become the dominant components. We illustrate this variation in flow patterns quantitatively in Figure 2dvii. For instance, as plasma β increases, the mean $V_{\perp y}$ changes from zero to primarily duskward and the interquartile range (Q3-Q1) narrows. In fact, at distance closest to the neutral sheet (Figure 2c, v-vi), both Q3 and Q1 are in the duskward regime. This indicates that the tailward flows near the neutral sheet are dominantly duskward (more dominant than the earthward flows in the same proxy of distance, see Figure 2bvi).

Summary: In brief, the variation in flow patterns in the XY plane is also observable in the YZ plane. For both earthward and tailward flows, as distance becomes closer to the neutral sheet, duskward flows become the dominant components and the strength of the flow deviation from the midnight plane weakens.

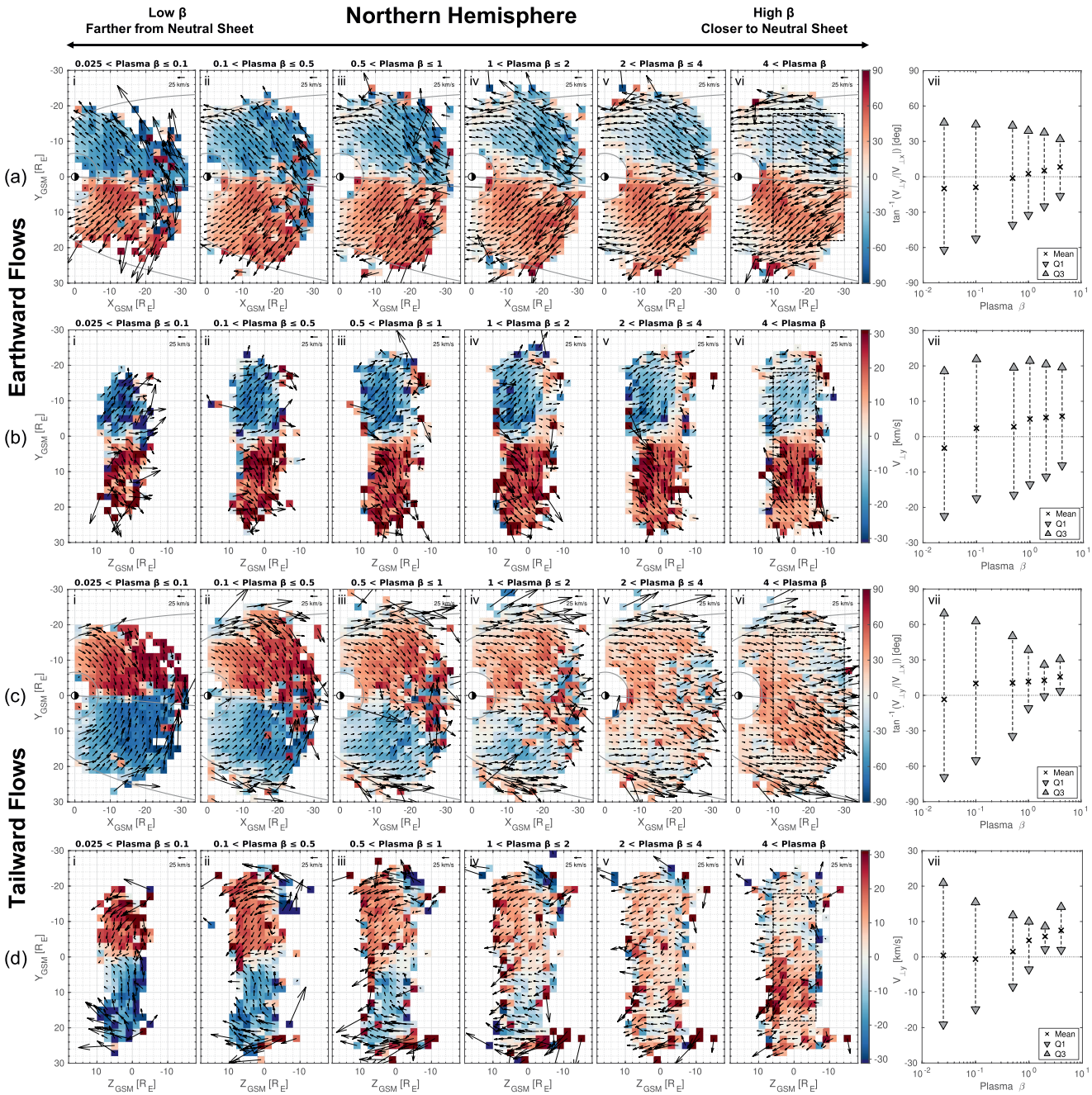

Figure 3. Descriptions are same as Figure 2 but only considering the ion flows that are in the Northern hemisphere (i.e., $B_x > 0$ nT).

4.3. Hemispheric Dependence

Based on the sign of B_x, we have also conducted similar analyses to Figure 2 but categorizing the data into Northern ($B_x > 0$ nT) and Southern ($B_x < 0$ nT) hemispheres. We show the results in Figures 3 and 4 respectively. In the XY plane, the variations in flow patterns in both hemispheres for both earthward and tailward flows are similar. They are consistent with the overall variations in flow patterns reported in Section 4.1 (where hemispheres are not differentiated). In the YZ plane, in the Northern hemisphere (i.e., Figures 3b and 3d), on average, the north-south flow component ($V_{\perp z}$) of the earthward (tailward) flows is southward (northward). The opposite is also true for Southern hemisphere (i.e., Figures 4b and 4d). Despite the changes in the direction of $V_{\perp z}$, the increasing dominance of duskward flows as the distance becomes closer to the neutral sheet for both earthward and tailward

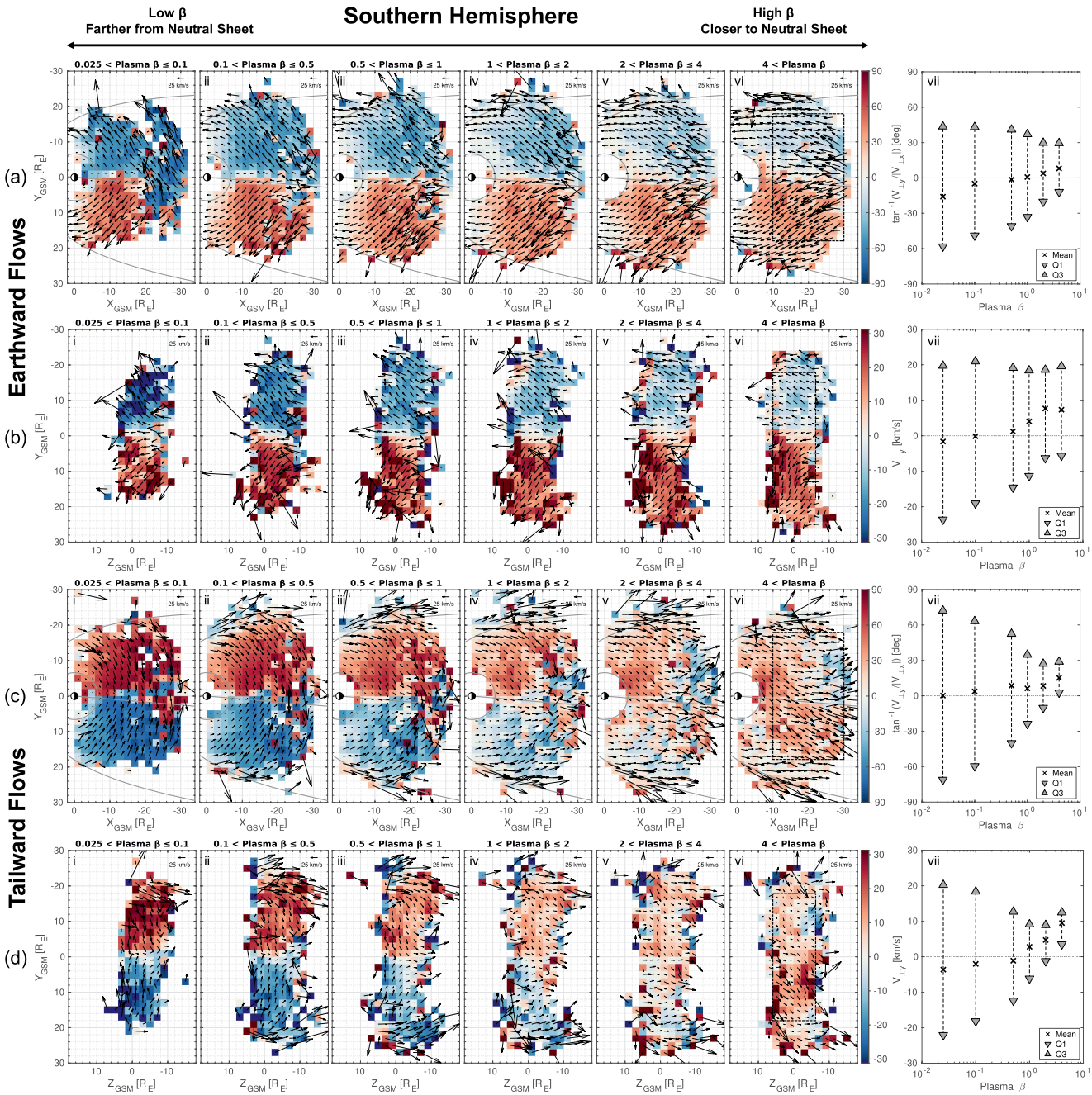

Figure 4. Descriptions are same as Figure 2 but only considering the ion flows that are in the Southern hemisphere (i.e., $B_x < 0$ nT).

flows is still observable in both hemispheres. In brief, we find that the ion flow patterns reported above are not hemispherically dependent.

5. Discussion

Different plasma instruments (onboard different missions) have different energy ranges and resolutions (see Section 2). Therefore, combining data across different instruments can introduce inconsistencies when we categorize the ion data based on plasma β. However, we have conducted the same analyses as Section 4 using individual missions (results not shown). We find that the overall variations in $V_{\perp x,y,z}$ which result in different flow patterns (as observable in Figures 2–4) are consistent across all missions.

Earth's magnetic field configuration in the magnetotail is dipolar and highly stretched. Ideally, closer to the neutral sheet (i.e., high plasma β), B_z is more dominant and $V_{\perp z}$ is therefore insignificant. As the distance becomes farther from the neutral sheet (i.e., low plasma β), B_z becomes less dominant and $V_{\perp z}$ becomes more significant. This variation in $V_{\perp z}$ with distance to the neutral sheet is evident for earthward and tailward flows respectively (see Figures 2b and 2d). Despite the increased significance in $V_{\perp z}$, our results show that the role of $V_{\perp y}$ in characterizing the flow patterns is also significant and should not be disregarded, even at a distance far from the neutral sheet. That is, the earthward and tailward flows diverge and converge with respect to the midnight plane quasi-symmetrically (e.g., Figures 2a and ci).

The flow patterns in Figures 1a–1d represent the average earthward and tailward flows in the magnetotail's plasma sheet, consistent with previous studies (e.g., Angelopoulos et al., 1993; Hori et al., 2000; Juusola, Østgaard, & Tanskanen, 2011; Kissinger et al., 2012; Paterson et al., 1998; Pitkänen et al., 2019; Wang et al., 2006). On average, the earthward (tailward) flows diverge from (converge toward) the midnight plane. However, our study finds that these flow patterns are not representative of all regions within the plasma sheet. As the distance changes from "farther from" to "closer to" the neutral sheet, there are two particular observations on the variations in ion flow patterns in the plasma sheet that we would like to highlight. We will refer them as Observation (1) and (2) respectively hereon. Observation (1): the flow divergence and convergence for earthward and tailward flows with respect to the midnight plane, respectively, become weaker. Observation (2): duskward flows become the dominant components. We suggest that these characteristic variations are likely due to the variations in the distribution of the electric ($\mathbf{V}_E$) and diamagnetic drift ($\mathbf{V}_{dia}$) with distance to the neutral sheet. In a two-fluid approximation, assuming isotropic plasmas in the plasma sheet, ion $\mathbf{V}_\perp$ can be described by the summation of $\mathbf{V}_E$ and $\mathbf{V}_{dia}$, where $\mathbf{V}_E = (\mathbf{E} \times \mathbf{B})/B^2$ and $\mathbf{V}_{dia} = (\mathbf{B} \times \nabla P)/(qn_iB^2)$. $\mathbf{E}$, $\mathbf{B}$, P, n_i and q are the electric field, magnetic field, ion pressure, ion number density and ion charge. $\mathbf{V}_E$ and $\mathbf{V}_{dia}$ describe the motions of low and high energy ions respectively. We refer the readers to previous works (e.g., Hori et al., 2000; Miyashita et al., 2020; Wang et al., 2006) for a better visualization of the average vector profiles of $\mathbf{V}_E$ and $\mathbf{V}_{dia}$.

On average, the electric field in the magnetotail is predominantly cross-tail ($\mathbf{E} = E_y\,\hat{\mathbf{y}}$), but has a notable (and small) Sun-Earth component with increasing distance from the midnight plane. As a result, $\mathbf{V}_E$ is directed mainly along the Sun-Earth line with small dawn-dusk component. This can describe the slightly diverging earthward (converging tailward) flows with respect to the midnight plane at distance close to the neutral sheet (i.e., Figures 2a–2dvi). As the distance becomes farther from the neutral sheet, E_z becomes the major component (Huang & Frank, 1994). As a result, the dawn-dusk component of the resulted $\mathbf{V}_E$ become more significant. Thus, this can describe the highly diverging earthward and converging tailward flows with respect to the midnight plane at distance farther from the neutral sheet (i.e., Figures 2a–2di). This variation of $\mathbf{V}_E$ with distance to the neutral sheet can explain Observation (1). Note that the variations in the vector profiles of $\mathbf{E}$ with distance to the neutral sheet have not been explored before. With more reliable electric field data from MMS missions, future works should investigate this further.

On average, due to the radially inward (earthward) ion pressure gradient, $\mathbf{V}_{dia}$ is directed mainly duskward (or westward). $\mathbf{V}_{dia}$ has a non-negligible but insignificant Sun-Earth component with increasing distance from the midnight plane. Based on the results in this study, we postulate that the contribution of overall $\mathbf{V}_{dia}$ varies with distance to the neutral sheet. For instance, as distance becomes closer the neutral sheet, the contribution of $\mathbf{V}_{dia}$ to the ion flows increases. This variation of $\mathbf{V}_{dia}$ with distance to the neutral sheet can explain Observation (2). The varying roles of $\mathbf{V}_{dia}$ with distance to the neutral sheet is not an established understanding. We emphasize that the validation of this hypothesis would require further investigations. $\mathbf{V}_{dia}$ depends on $\mathbf{B}$, P and n_i. Future works should investigate the relationship between $\mathbf{B}$, P and n_i in causing the varying $\mathbf{V}_{dia}$ with distance to the neutral sheet.

As the distance becomes closer to the neutral sheet, the increasing dominance of the duskward $\mathbf{V}_{dia}$ can explain the gradual diminishing of the dawnward flow components in the dawnside (duskside) of the plasma sheet for earthward (tailward) flows (see Figures 2a and 2ci–vi). However, the increasing dominance of the duskward $\mathbf{V}_{dia}$ solely cannot explain the gradual diminishing of the duskward flow components in the duskside (dawnside) of the plasma sheet for earthward (tailward) flows. Note that the strength of both dawnward and duskward flow components decreases as the distance becomes closer to the neutral sheet. However, the strength of dawnward flows decreases more rapidly than the duskward flows. This is applicable for both earthward and tailward flows (see Figures 2a–2d, i–vi). It is this asymmetry in the decreases of flow strength that results in duskward flows in

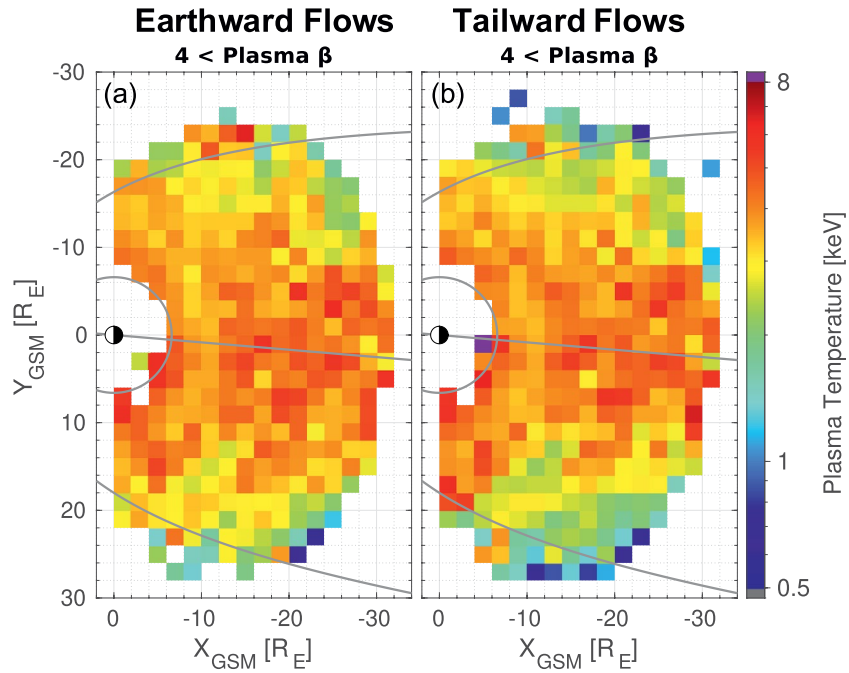

Figure 5. The spatial distribution of average ion temperature for (a) earthward and (b) tailward flows respectively in the XY plane. Only high plasma β ions (i.e., $\beta > 4$) are considered.

becoming the dominant components as the distance becomes closer to the neutral sheet. Therefore, Observations (1) and (2) are due to the combined varying effects of $\mathbf{V}_E$ and $\mathbf{V}_{dia}$, and cannot be due to just $\mathbf{V}_{dia}$.

Previous studies on magnetotail's plasma sheet (e.g., Angelopoulos et al. (1993); Hori et al. (2000); Wang et al. (2006)) computed the average flows irrespective of the direction. These studies reveal that the overall net flows are slow (<200 km/s) and earthward. In contrast, our study categorizes the ion flows into earthward and tailward components. This approach allows us to investigate if the variation in flow patterns with distance to the neutral sheet is consistent between earthward and tailward flows. We find that both earthward and tailward flows are similarly subjected to the varying effects of $\mathbf{V}_E$ and $\mathbf{V}_{dia}$ with distance to the neutral sheet. However, these effects are applicable to different extents depending on the flow directions. For instance, at distance closest to the neutral sheet, the dominance of duskward flow components on the tailward flows is more prominent when compared to the earthward flows (see Figures 2a–2dvi). One explanation could be because of the difference in the average ion energy between earthward and tailward flows. The motion of low and high energy ions can be described by $\mathbf{V}_E$ and $\mathbf{V}_{dia}$, respectively (Chen, 1984; Juusola, Østgaard, & Tanskanen, 2011). In other words, it is possible that in our data set, the plasma energy of the tailward flows with high plasma β is on average higher than the earthward flows with high plasma β. However, further analyses indicate that this is not the case. We show the spatial distribution of average ion temperature for earthward and tailward flows respectively in Figures 5a–5b. Results show that at distance closer to the neutral sheet (i.e., ion with plasma $\beta > 4$), both earthward and tailward flows have similar spatial distribution of ion temperature. Therefore, the difference in the average ion energy between earthward and tailward flows cannot explain the dominance of duskward flows on tailward flows at distance closer to the neutral sheet. This dominance of duskward flows on tailward flows (more dominant than earthward flows) at distance closer to the neutral sheet deserves further attention in future works.

The flow behaviors reported in this study reveal that the magnetotail flows are even more complex than what we previously understood. It changes the traditional picture of the simple steady convection (Dungey, 1961) we have on the plasma sheet. This study raises a number of consequential questions: Are the convection behaviors consistent between different plasma species (e.g., ions and electrons) and between different ion species (e.g., protons and heavy ions)? What are the implications if they are/are not? Follow-up works and answers to these questions are necessary to better understand the dynamics of the complex magnetotail flows. Our study can be viewed as a stepping stone to future studies in this aspect.

6. Conclusion

In conclusion, we present a work that, for the first time, explores the slow (<200 km/s) ion flow patterns as a function of the distance to the neutral sheet. By using plasma β as a proxy of distance to the neutral sheet, we find that the ion flow patterns vary systematically within the plasma sheet. As the distance becomes closer toward the neutral sheet, the strength of the earthward (tailward) flows divergence (convergence) with respect to the midnight plane weakens and duskward flows become the dominant components. We also find that the variations in ion flow patterns are not hemispherically dependent. We suggest that the spatial profiles of the electric and diamagnetic drift vary with distance to the neutral sheet and are therefore responsible for the varying ion flow patterns.

Data Availability Statement

Geotail data are available from DARTS at Institute of Space and Astronautical Science, https://darts.isas.jaxa.jp/. THEMIS data are available from CDAWeb, https://cdaweb.sci.gsfc.nasa.gov/index.html/. Cluster data are available from Cluster Science Archive, https://www.cosmos.esa.int/web/csa. MMS data are available from MMS Science Data Center, https://lasp.colorado.edu/mms/sdc/public/.

Acknowledgments
The authors would like to thank all the Geotail, THEMIS, Cluster and MMS team members for the successful operation of the instrument and the calibration of the data. Particularly, we would like to acknowledge T. Nagai (Geotail MGF), Y. Saito (Geotail LEP), E. Lucek (Cluster FGM), I. Dandouras (Cluster CIS), C. Russell (MMS FGM) and B. Giles (MMS FPI). We acknowledge NASA contract NAS5-02 099 and V. Angelopoulos for use of data from the THEMIS Mission. Specifically, we would like to thank C. W. Carlson and J. P. McFadden for the use of ESA data and K. H. Glassmeier, U. Auster and W. Baumjohann for the use of FGM data provided under the lead of the Technical University of Braunschweig and with financial support through the German Ministry for Economy and Technology and the German Center for Aviation and Space (DLR) under contract 50 OC 0302. GS. Chong would like to acknowledge Dr. Andrew Walsh and Dr. Anita Kullen for their helpful comments on this work. Participants from Umeå University received financial assistance from the Swedish National Space Agency (SNSA) Grant 81/17 (GS. Chong), 118/17 (T. Pitkänen) and 217/14 (M. Hamrin).

References

Angelopoulos, V., Baumjohann, W., Kennel, C. F., Coronti, F. V., Kivelson, M. G., Pellat, R., et al. (1992). Bursty Bulk flows in the inner central plasma sheet. *Journal of Geophysical Research*, *97*(A4), 4027–4039. https://doi.org/10.1029/91JA02701

Angelopoulos, V., Kennel, C. F., Coroniti, F. V., Pellat, R., Kivelson, M. G., Walker, R. J., et al. (1994). Statistical characteristics of bursty bulk flow events. *Journal of Geophysical Research*, *99*(A11), 21257–21280. https://doi.org/10.1029/94JA01263

Angelopoulos, V., Kennel, C. F., Coroniti, F. V., Pellat, R., Spence, H. E., Kivelson, M. G., et al. (1993). Characteristics of ion flow in the quiet state of the inner plasma sheet. *Geophysical Research Letters*, *20*(16), 1711–1714. https://doi.org/10.1029/93GL00847

Auster, H. U., Glassmeier, K. H., Magnes, W., Aydogar, O., Baumjohann, W., Constantinescu, D., et al. (2008). The THEMIS fluxgate magnetometer. *Space Science Reviews*, *141*(1–4), 235–264. https://doi.org/10.1007/s11214-008-9365-9

Balogh, A., Carr, C. M., Acuña, M. H., Dunlop, M. W., Beek, T. J., Brown, P., et al. (2001). The Cluster Magnetic Field Investigation: Overview of in-flight performance and initial results. *Annales Geophysicae*, *19*(10), 1207–1217. https://doi.org/10.5194/angeo-19-1207-2001

Baumjohann, W., Paschmann, G., & Luehr, H. (1990). Characteristics of high-speed ion flows in the plasma sheet. *Journal of Geophysical Research*, *95*(A4), 3801–3809. https://doi.org/10.1029/JA095iA04p03801

Baumjohann, W., Paschmann, G., Sckopke, N., Cattell, C. A., & Carlson, C. W. (1988). Average ion moments in the plasma sheet boundary layer. *Journal of Geophysical Research*, *93*(A10), 11507–11520. https://doi.org/10.1029/JA093iA10p11507

Boakes, P., Nakamura, R., Volwerk, M., & Milan, S. (2014). Eclat cluster spacecraft magnetotail plasma region identifications (2001–2009). *Dataset Papers in Science*, *2014*, 1–13. https://doi.org/10.1155/2014/684305

Chen, F. F. (1984). *Introduction to plasma physics and controlled fusion* (Vol. 1). Springer.

Decoster, R. J., & Frank, L. A. (1979). Observations pertaining to the dynamics of the plasma sheet. *Journal of Geophysical Research*, *84*(A9), 5099–5120. https://doi.org/10.1029/JA084iA09p05099

Dungey, J. W. (1961). Interplanetary magnetic field and the auroral zones. *Physical Review Letters*, *6*(2), 47–48. https://doi.org/10.1103/PhysRevLett.6.47

Haaland, S., Lybekk, B., Maes, L., Laundal, K., Pedersen, A., Tenfjord, P., et al. (2017). North-south asymmetries in cold plasma density in the magnetotail lobes: Cluster observations. *Journal of Geophysical Research*, *122*(1), 136–149. https://doi.org/10.1002/2016JA023404

Hamrin, M., Norqvist, P., Marghitu, O., Buchert, S., Klecker, B., Kistler, L. M., & Dandouras, I. (2009). Occurrence and location of concentrated load and generator regions observed by Cluster in the plasma sheet. *Annales Geophysicae*, *27*(11), 4131–4146. https://doi.org/10.5194/angeo-27-4131-2009

Hones, E. W. Jr. (1979). Transient Phenomena in the Magnetotail and Their Relation to Substorms (Article published in the special issues: Proceedings of the Symposium on Solar Terrestrial Physics held in Innsbruck, May- June 1978. *Space Science Reviews*, *23*(3), 393–410. https://doi.org/10.1007/BF00172247

Hori, T., Maezawa, K., Saito, Y., & Mukai, T. (2000). Average profile of ion flow and convection electric field in the near-Earth plasma sheet. *Geophysical Research Letters*, *27*(11), 1623–1626. https://doi.org/10.1029/1999GL003737

Huang, C. Y., & Frank, L. A. (1994). A statistical survey of the central plasma sheet. *Journal of Geophysical Research*, *99*(A1), 83–96. https://doi.org/10.1029/93JA01894

Juusola, L., Østgaard, N., & Tanskanen, E. (2011). Statistics of plasma sheet convection. *Journal of Geophysical Research*, *116*(A8), A08201. https://doi.org/10.1029/2011JA016479

Juusola, L., Østgaard, N., Tanskanen, E., Partamies, N., & Snekvik, K. (2011). Earthward plasma sheet flows during substorm phases. *Journal of Geophysical Research*, *116*(A10), A10228. https://doi.org/10.1029/2011JA016852

Kissinger, J., McPherron, R. L., Hsu, T. S., & Angelopoulos, V. (2012). Diversion of plasma due to high pressure in the inner magnetosphere during steady magnetospheric convection. *Journal of Geophysical Research*, *117*(A5), A05206. https://doi.org/10.1029/2012JA017579

Kokubun, S., Yamamoto, T., Acuña, M. H., Hayashi, K., Shiokawa, K., & Kawano, H. (1994). The GEOTAIL magnetic field experiment. *Journal of Geomagnetism and Geoelectricity*, *46*(1), 7–21. https://doi.org/10.5636/jgg.46.7

McFadden, J. P., Carlson, C. W., Larson, D., Ludlam, M., Abiad, R., Elliott, B., et al. (2008). The THEMIS ESA plasma instrument and in-flight calibration. *Space Science Reviews*, *141*(1–4), 277–302. https://doi.org/10.1007/s11214-008-9440-2

McPherron, R. L., Hsu, T. S., Kissinger, J., Chu, X., & Angelopoulos, V. (2011). Characteristics of plasma flows at the inner edge of the plasma sheet. *Journal of Geophysical Research (Space Physics)*, *116*, A00I33. https://doi.org/10.1029/2010JA015923

Miyashita, Y., Seki, K., Sakaguchi, K., Hiraki, Y., Nosé, M., Machida, S., et al. (2020). On the transition between the inner and outer plasma sheet in the Earth's Magnetotail. *Journal of Geophysical Research*, *125*(4), e27561. https://doi.org/10.1029/2019JA027561

Mukai, T., Machida, S., Saito, Y., Hirahara, M., Terasawa, T., Kaya, N., et al. (1994). The Low Energy Particle (LEP) Experiment onboard the GEOTAIL Satellite. *Journal of Geomagnetism and Geoelectricity*, *46*(8), 669–692. https://doi.org/10.5636/jgg.46.669

Nagai, T., Fujimoto, M., Nakamura, R., Saito, Y., Mukai, T., Yamamoto, T., et al. (1998). Geotail observations of a fast tailward flow at $X_{GSM} = -15R_E$. *Journal of Geophysical Research*, *103*(A10), 23543–23550. https://doi.org/10.1029/98JA02246

Nakamura, R., Baker, D. N., Fairfield, D. H., Mitchell, D. G., McPherron, R. L., Hones, E. W. Jr. (1994). Plasma flow and magnetic field characteristics near the midtail neutral sheet. *Journal of Geophysical Research*, *99*(A12), 23591–23602. https://doi.org/10.1029/94JA02082

Nilsson, H., Hamrin, M., Pitkänen, T., Karlsson, T., Slapak, R., Andersson, L., et al. (2016). Oxygen ion response to proton bursty bulk flows. *Journal of Geophysical Research*, *121*(8), 7535–7546. https://doi.org/10.1002/2016JA022498

Ohtani, S., Miyashita, Y., Singer, H., & Mukai, T. (2009). Tailward flows with positive B_Z in the near-Earth plasma sheet. *Journal of Geophysical Research*, *114*, A06218. https://doi.org/10.1029/2009JA014159

Paterson, W. R., Frank, L. A., Kokubun, S., & Yamamoto, T. (1998). Geotail survey of ion flow in the plasma sheet: Observations between 10 and $50R_E$. *Journal of Geophysical Research*, *103*(A6), 11811–11825. https://doi.org/10.1029/97JA02881

Pitkänen, T., Kullen, A., Laundal, K. M., Tenfjord, P., Shi, Q. Q., Park, J. S., et al. (2019). IMF B_y influence on Magnetospheric convection in Earth's Magnetotail Plasma Sheet. *Geophysical Research Letters*, *46*(21), 11698–11708. https://doi.org/10.1029/2019GL084190

Pollock, C., Moore, T., Jacques, A., Burch, J., Gliese, U., Saito, Y., et al. (2016). Fast plasma investigation for Magnetospheric multiscale. *Space Science Reviews*, *199*(1–4), 331–406. https://doi.org/10.1007/s11214-016-0245-4

Raj, A., Phan, T., Lin, R. P., & Angelopoulos, V. (2002). Wind survey of high-speed bulk flows and field-aligned beams in the near-Earth plasma sheet. *Journal of Geophysical Research*, *107*(A12), 1419. https://doi.org/10.1029/2001JA007547

Rème, H., Aoustin, C., Bosqued, J. M., Dand ouras, I., Lavraud, B., Sauvaud, J. A., et al. (2001). First multispacecraft ion measurements in and near the Earth's magnetosphere with the identical Cluster ion spectrometry (CIS) experiment. *Annales Geophysicae*, *19*, 1303–1354. https://doi.org/10.5194/angeo-19-1303-2001

Russell, C. T., Anderson, B. J., Baumjohann, W., Bromund, K. R., Dearborn, D., Fischer, D., et al. (2016). The magnetospheric multiscale magnetometers. *Space Science Reviews*, *199*(1–4), 189–256. https://doi.org/10.1007/s11214-014-0057-3

Schödel, R., Baumjohann, W., Nakamura, R., Sergeev, V. A., & Mukai, T. (2001). Rapid flux transport in the central plasma sheet. *Journal of Geophysical Research*, *106*(A1), 301–313. https://doi.org/10.1029/2000JA900139

Schödel, R., Nakamura, R., Baumjohann, W., & Mukai, T. (2001). Rapid flux transport and plasma sheet reconfiguration. *Journal of Geophysical Research*, *106*(A5), 8381–8390. https://doi.org/10.1029/2000JA900159

Shue, J. H., Chao, J. K., Fu, H. C., Russell, C. T., Song, P., Khurana, K. K., & Singer, H. J. (1997). A new functional form to study the solar wind control of the magnetopause size and shape. *Journal of Geophysical Research*, *102*(A5), 9497–9511. https://doi.org/10.1029/97JA00196

Takahashi, K., Hones, E. W. Jr. (1988). ISEE 1 and 2 observations of ion distributions at the plasma sheet-tail lobe boundary. *Journal of Geophysical Research*, *93*(A8), 8558–8582. https://doi.org/10.1029/JA093iA08p08558

Wang, C.-P., Lyons, L. R., Weygand, J. M., Nagai, T., & McEntire, R. W. (2006). Equatorial distributions of the plasma sheet ions, their electric and magnetic drifts, and magnetic fields under different interplanetary magnetic field B_z conditions. *Journal of Geophysical Research*, *111*(A4), A04215. https://doi.org/10.1029/2005JA011545

Zhang, L. Q., Baumjohann, W., Wang, J. Y., Rème, H., Dunlop, M. W., & Chen, T. (2015). Statistical characteristics of slow earthward and tailward flows in the plasma sheet. *Journal of Geophysical Research: Space Physics*, *120*(8), 6199–6206. https://doi.org/10.1002/2015JA021354

Zhang, L. Q., Wang, J. Y., Baumjohann, W., Rème, H., & Dunlop, M. W. (2015). Earthward and tailward flows in the plasma sheet. *Journal of Geophysical Research: Space Physics*, *120*, 4487–4495. https://doi.org/10.1002/2015JA021154